

Article citation info:

Pielecha I, Szwajca F, Experimental study and modelling of an air-cooled proton exchange membrane fuel cell stack in the static and dynamic performance, *Eksploracja i Niezawodność – Maintenance and Reliability* 2024: 26(2) <http://doi.org/10.17531/ein/184232>

Experimental study and modeling of an air-cooled proton exchange membrane fuel cell stack in the static and dynamic performance

Indexed by:



Ireneusz Pielecha^{a,*}, Filip Szwajca^a

^a Poznan University of Technology, Poland

Highlights

- Fuel Cell Stack Under Static and Dynamic Load.
- Sankey Diagram Analysis for Fuel Cell Stack.
- Higher Efficiency of a Static Load Condition Fuel Cell Stack.
- Modeling of Fuel Cell Loading under Static and Dynamic Conditions.
- Better Accuracy of Models for Static Loading Conditions.

Abstract

Research on Proton Exchange Membrane fuel cells is an important area in the field of modern energy sources. Such fuel cells are characterized by high efficiency and fast response times, making them a promising solution for sustainable energy production. Fuel cells operate under both static and dynamic conditions. Such varying operating conditions result in achieving different efficiency of fuel cell systems. This study attempts an experimental and modeled efficiency evaluation of a 1.2 kW open-cathode air-cooled fuel cell stack under static and dynamic conditions. A Sankey energy balance and an analysis of the balance components were determined for the fuel cell stack operating in these two operating states. Simultaneous modeling of the fuel cell under both static and dynamic conditions was carried out. The efficiency values of the fuel cell stack were found to be slightly higher under static conditions than under dynamic conditions. Modeling fuel cells in static and dynamic conditions results in slightly different parameters (better conformance was obtained for static models).

Keywords

fuel cell system, static and dynamic condition, fuel cell modeling

This is an open access article under the CC BY license (<https://creativecommons.org/licenses/by/4.0/>)

1. Introduction

Research on Proton Exchange Membrane (PEM) fuel cells is an important area in the field of modern energy sources. Such fuel cells are characterized by high efficiency and fast response times, making them a promising solution for sustainable energy production. PEM fuel cells are utilized in three primary domains: transportation, stationary applications, and portable applications [1]. The key determinant that influences the selection of a fuel cell application is the generated power. Presently, PEM fuel cells find application in the mentioned sectors, with power outputs spanning a broad range from a few hundred watts for E-Bikes or drones [2, 3], to several hundred kilowatts for locomotives, ships or

stationary power generators [4, 5, 6].

One of the key aspects of testing PEM cells is analyzing the operational conditions that significantly impact their performance and durability. These conditions include temperature, humidity, pressure, fuel and airflow, as well as electrical load conditions and intensity.

2. Current Research Status of PEM Fuel Cells

The characteristics of systems equipped with fuel cells can be analyzed under both static and dynamic loading conditions. Hoeflinger et al. [7] tested a bench equipped with a 30 kW PEM fuel cell stack and analyzed the effect of pressure and

(*) Corresponding author.

E-mail addresses:

I. Pielecha, (ORCID: 0000-0001-7340-635X) ireneusz.pielecha@put.poznan.pl, F. Szwajca (ORCID: 0000-0001-5724-0927) filip.szwajca@put.poznan.pl,

the mass of air supplied to the cathode on the cell's operation under static conditions. Experimental work was carried out for a load in the range of 120–400 A, while a model study was conducted for a load of 500 A. For high loads, higher efficiency was obtained by increasing the pressure of the supplied air and reducing the mass flow rate. For smaller loads, the tendency is the opposite: it is beneficial to increase the mass flow rate of air and reduce the air pressure. The study was conducted for an excess air ratio λ in the range of 1.35–2.4. As a result, the studied system had a maximum efficiency of 55.21% for the smallest analyzed load (120 A) and 43.74% for 400 A. Another paper [8] presented the positive effect of increasing the inlet air pressure from 1.2 to 1.5 bar for a 1 kW cell, causing voltage increases over the entire analyzed current density range from 0–600 mA/cm² on the polarization curve.

The authors of another study [9] conducted tests on a 1 kW PEM fuel cell stack under dynamic and static conditions, considering two hydrogen delivery pressures of 0.6 and 0.8 atm, as specified by the manufacturer as optimal. In the static approach, the load was incrementally changed from 0 to 22 A, in steps of 1 A, for tests lasting 60 seconds each. The hydrogen delivery pressure was found to have no effect on specific fuel consumption, although notable differences in volumetric consumption were observed. The highest efficiency, nearly 45%, was achieved under a 9 A load and a 0.6 atm supply pressure. Dynamic state tests involved dynamically varying the load from an initial value to a predetermined final value for different ranges: 0–4 A, 8–12 A, 10–14 A, 18–22 A, and 20–22 A. This type of testing enabled the analysis of transient responses and the determination of the instantaneous power consumption of auxiliary systems, such as a ventilator.

Water management was analyzed by testing a single-cell open-cathode PEM fuel cell with an effective area of 16 cm² [10]. Polarization curves were determined by varying the cell voltage from open circuit to the maximum load where the voltage reached 0.2 V. The load value was adjusted at a rate of 1 mV/s. It was demonstrated that under low-load conditions, membrane dehydration occurs, resulting in uneven water distribution. As the load increases, the water content rises significantly, which can lead to the accumulation of liquid

water.

The performance of single PEM cells with various designs (effective area of 5 cm² and 25 cm²) and a fuel cell stack comprising eight 49 cm² membranes was investigated through both dynamic and static loading [11]. The impact of operational factors, including temperature, humidity, gas stoichiometry, and pressure, was assessed under static conditions. Subsequently, the influence of these same conditions on the fuel cell's response was studied under varying loads, with a stepwise progression of initial increase followed by successive decrease, and according to a profile featuring irregular current spikes. The dynamic tests varied in duration from 300 to over 1,300 seconds. The most unfavorable response to dynamic loading was observed for an air stoichiometry of 1, cathode gas pressure at 1 atm, and a cell with a single serpentine flow pattern. On the other hand, the most favorable outcomes were achieved with a cell featuring parallel flow and a triple serpentine flow pattern

Under constant operating conditions, the response of a system equipped with two stacks of 1.2 kW fuel cells to dynamic loading was analyzed [12]. By dynamically varying the load from open circuit to 15 A within a span of several milliseconds, the maximum discrepancy between the load and the cell response was 7.5 A. When employing a semi-sinusoidal load profile with an amplitude also of 15 A and a period of 1 second, a smaller difference between the input and output signals, not exceeding 2 A, was achieved.

Studying a PEM-type fuel cell with an active area of 25 cm², Chandran et al. [13] examined the impact of dynamic loading on its degradation. The tests were conducted for a total of 2,000 cycles or until the initial performance decreased by 10 percent or more, employing two loading profiles that differed in their rate of load build-up. After every 100 cycles, a polarization curve and electrochemical impedance spectroscopy (EIS) analysis were performed, and the cell components underwent field emission scanning electron microscopy (FESEM) imaging upon completing the entire test. The degradation reached 20.67 percent and 10.72 percent for the tests with lower and higher load build-up rates, respectively. The relationship between degradation, cycle count, and load change rate was established. Attention was also directed towards fuel cell degradation during start-up and

shutdown, attributed to the reverse current mechanism, which manifested through harsh corrosion conditions in the cathode layer [14]. The impact of fuel cell temperature and relative humidity on degradation was also investigated under the most severe cycling on-off conditions [15]. With a consistent relative humidity, degradation rates declined as temperature decreased. A humidity level of approximately 70 percent emerged as the most favorable in terms of durability and operation at the lowest feasible temperature, thereby enabling efficient fuel cell performance.

In a study concerning fuel cell start-up [16], it was demonstrated that the cell couldn't be effectively loaded during the initial activation phase when the current step was increased from zero to 0.8 A/cm²; however, after activation, the load could be increased to 1.5 A/cm². The assessment was carried out by incrementally raising the current, and the measured voltage served as an indicator of dynamic performance.

The impact of supplying the fuel cell with oxygen-enriched air during static operation was also investigated [17]. The experiments were performed using three cells connected in series, each having an active area of 50 cm². The air was enriched with oxygen in the range of 23 to 50%, resulting in voltage outputs of 2.52 V and 2.80 V, respectively. Considering the other operational parameters of the cell, the optimal oxygen content was found to be 45%, leading to a 9% increase in voltage efficiency and a 33% boost in power output.

The behavior of a high-power system equipped with a PEM fuel cell stack rated at 100 kW, with a current density of 1.4 A/cm², and used in vehicles, was analyzed during start-up at -30°C [18]. The start-up process lasted 110 seconds, during which 50% of the system's rated power was attained, and the temperature increased to below 40°C. Emphasis was placed on the significance of the rapid stack temperature rise and the limited impact of low temperature on the system activation's success. The overall efficiency of the system was scrutinized, with a higher value observed for the fuel cell stack operating alone across the entire operational range. For open circuit conditions, it was 78.9%, and when subjected to a load, it decreased to 53.8%. As for the entire system, the maximum efficiency reached 55.41%, dropping to 44.5%

under maximum load.

The efficiency results of the stack operating individually and within the system, with various compressor efficiency and cathode stoichiometry values, along with air pressure set at 2.0 and 2.2 bar, were presented by Walters et al. [19]. The maximum efficiency value for the stack alone slightly exceeded 50%, while for the system, it hovered around 45%, assuming 100% compressor efficiency at an air pressure of 2.2 bar. As compressor efficiency diminishes, the overall system efficiency also decreases. The reduction in the overall system efficiency in comparison to the stack, due to compressor losses or inappropriate operating temperatures, among other factors, was highlighted by Vidovic et al. [20].

The proportion of energy consumed by the Balance of Plant (BoP) is noteworthy. Tests conducted on a Hyundai Nexo hydrogen vehicle under steady-state conditions revealed an energy consumption of a 9.1 kWe compressor, within a system rated at 82 kWe and possessing an efficiency of 66.8% [21]. Depending on the specific system and the type of power converter used, it is generally characterized by an efficiency exceeding 97% [22]. An examination of a 100 kW generator system incorporating ultracapacitors for energy storage demonstrated that at a load of 45 kW, the efficiency of DC/AC power conversion using a prototype converter reached 96.2%, and for an 80 kW load, it was 94.9% [23]. In a system equipped with a 5 kW cell, operating within a load range of 0.3 kW to 1.6 kW, the efficiency of the DC/DC converter ranged from 97% to 98% [24].

3. The Aim of the Study Proceedings

The investigation of fuel cells employed within FC vehicles beyond their inherent operational environment is a notably intricate subject. Consequently, it is evident that the conduction of both static and dynamic assessments on fuel cells is approached with consideration for their scalability. This particular concern constitutes the focal point addressed within the present study. The undertaking of research involving a cell module with an approximate power output of 1.2 kW stands to facilitate a gradual transition towards the realization of scalable, higher-capacity fuel cell systems over the long term. The antecedent section, dedicated to the state of the art, showcased outcomes from other researchers aimed at

the comprehensive appraisal of fuel cell performance across a spectrum of diverse testing protocols.

Within this paper, an examination was conducted on the energy indicators of a fuel cell stack, gleaned from the outcomes of subjecting it to both static and dynamic loading. Furthermore, a comprehensive energy balance analysis, represented in the form of a Sankey diagram, was executed, and concurrent fuel cell modeling endeavors were undertaken. These multifaceted procedures were orchestrated with the intent of characterizing the research potential inherent in high-power fuel cells operating under conditions characteristic of typical vehicle propulsion scenarios. The findings derived from these investigations will serve for the subsequent analysis and modeling of analogous systems.

4. Fuel Cell Modeling

Utilizing the Butler-Volmer equation [25], which correlates with the equilibrium potential of a fuel cell, it becomes possible to identify three distinct domains of voltage loss:

- voltage activation;
- resistive;
- mass transport.

The comprehensive equation encompassing all forms of voltage losses can be formulated as follows: On the voltage value of the fuel cell U_{FC} consists of the open collector voltage E_{OC} – overvoltage (activation losses) – U_{act} , ohmic voltage losses – U_{ohm} and losses of tension due to mass transport – U_{trans} :

$$U_{FC} = E_{OC} + U_{act} + U_{ohm} + U_{trans} \quad (1)$$

The above components are determined as follows:

- the voltage of the fuel cell with an open electrical circuit [26]:

$$E_{OC} = \frac{\Delta \bar{g}_f}{2 \cdot F} \quad (2)$$

where: $\Delta \bar{g}_f$ – Gibbs free energy, F – Faraday constant.

- the activation loss voltage U_{act} :

$$U_{act} = A \cdot \ln(i) \quad (3)$$

where: A – activation overvoltage, i – area-specific current (current density).

- resistive (ohmic) voltage losses U_{ohm} :

$$U_{ohm} = r \cdot i \quad (4)$$

where: r – area specific resistance (internal resistance).

- mass transport voltage losses U_{trans} :

$$U_{trans} = m \cdot \exp(n \cdot i) \quad (5)$$

where: m – constants in the mass-transfer overvoltage, n – constants in the mass-transfer overvoltage. Using all of the component equations (2)–(5), one can write:

$$U_{FC} = E_{OC} - A \cdot \ln(i) - r \cdot i - m \cdot \exp(n \cdot i) \quad (6)$$

Equation (6) is the basis for determining the voltage losses of a fuel cell.

5. Testing Methodology

5.1. Test Stand and Apparatus

The investigation was conducted employing a Hybrid Energy Lab-System founded upon a 1.2 kW air-cooled open-cathode PEM fuel cell stack (Fig. 1a). This stack comprises 36 cells, yielding voltages spanning the 18–36 V spectrum. The configuration integrates lead-acid batteries, possessing an energy capacity of 18 Ah and a voltage output of 24 V. Integrated within the system are a DC/DC voltage converter and a programmable load system. The experimentation harnessed a supply of hydrogen, stored within a steel cylinder at a maximum pressure of 20 MPa, subsequently regulated to a constant pressure of 5 bar before the valve of the fuel cell stack inlet (Fig. 1b). A comprehensive summary of the bench's technical specifications is presented in Table 1.

Table 1. Technical data of Hybrid Energy Lab-System [27].

Fuel cell		
Rated output	W	1200
Rated current	A	60
Operating voltage	V	18–36
Hydrogen purity	Min.	4.0
Permissible H ₂ inlet pressure	bar	1–15
DC converter		
Max output power	W	1500
Max output current	A _{DC}	55
Rated output voltage	V _{DC}	24
Output voltage range	V _{DC}	21–30
Max input current	A _{DC}	60
Input voltage range	V _{DC}	18–36
Efficiency	%	96
Inverter		
Continuous output power (50 Hz), 115 VAC (60Hz)	W _{AC}	1500
Inlet voltage	V _{DC}	21 ... 30
Output voltage	V _{AC}	230
Efficiency	%	93
Electronic Load Module		
Max continuous power	W	1200
DC load current	A _{DC}	0–85
DC load voltage	V _{DC}	0–80
Battery Module		
Battery set 1	lead-acid	24 V (2 x 12 V), 7.2 Ah
Battery set 2	lead-acid	24 V (2 x 12 V), 18 Ah

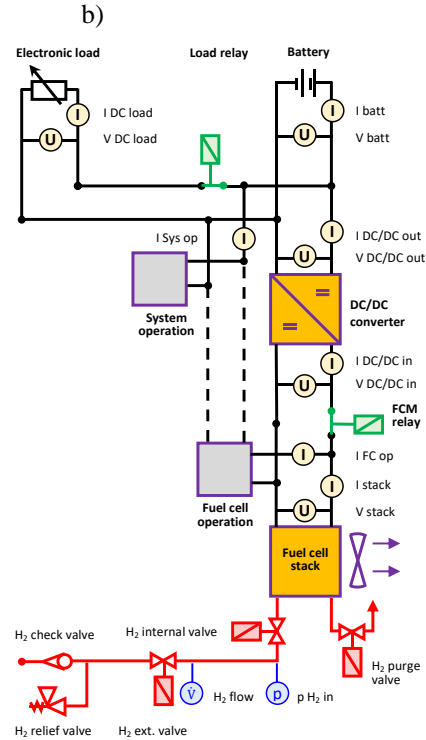
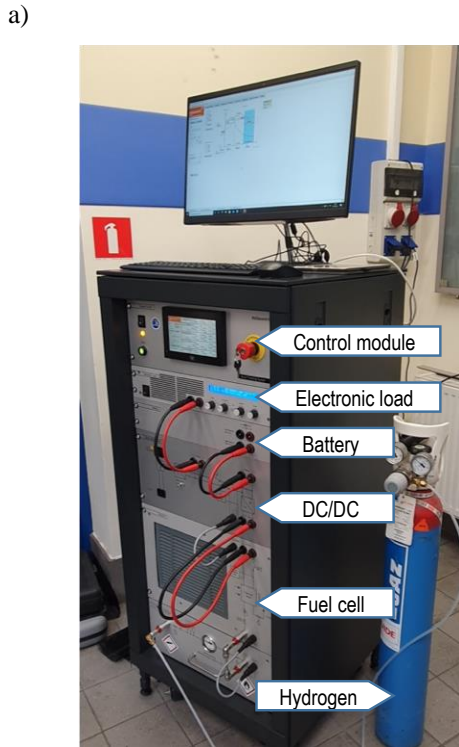


Fig. 1. Hybrid Energy Lab measurement system from Heliocentris: a) view, b) schematic of the system.

5.2. Scope of Research

The research undertaken was geared towards the comprehensive evaluation of performance characteristics exhibited by fuel cells when subjected to both static and dynamic loading scenarios while maintaining consistent parameters for both air and hydrogen streams. The pertinent parameters defining the current profiles for the examined cases are presented in Table 2. The precise depiction of the actual current profile is visually represented in Fig. 2, with the static cycle denoted by the green color and the dynamic cycle illustrated in red. Within the static profile, three instances of load variation were chosen, employing a time interval of 230 seconds for each ascending step. A comparable ramped load profile was employed in a prior study [28], serving as the basis for the validation of the fuel cell modeling algorithm. Subsequently, a dynamic profile was instituted, featuring load changes occurring at intervals of 3 seconds. The previously stepped profile was iterated three times (Fig. 2).

Table 2. Scope of research work.

Test type	Research test	Test time	Max stack load
Static + modeling	Statically rising load	622 s	0.93 kW
Dynamic + modeling	Dynamic rising load – three times repetition	538 s	1.13 kW

The static tests commenced with an initial load of approximately 13 A (within the scope of 12–15.7 A) at $t = 230$ s (Fig. 3). Subsequently, the load was augmented to around 27 A (ranging between 25–31.5 A). The terminal phase of the cycle was established at 38 A (falling within the span of 35–41 A). The test was concluded after a duration of 622 seconds.

Dynamic loading was designed in the format of incremental stepwise current increments over time intervals of $dt = 3$ s. The loading sequence commenced with an initial value of $I = 8$ A and progressively increased to 53 A. Subsequently, the load was reverted back to 8 A. This profile, spanning a duration of $t = 180$ s, was reiterated three times. The cumulative duration of the entire test amounted to 538 seconds.

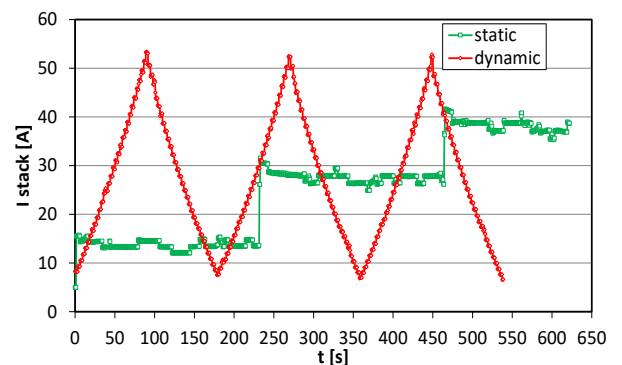


Fig. 2. Fuel cell load profile: static and dynamic.

The approach to modeling fuel cells, as elucidated in Chapter 3, was employed in the current study. The parameters compiled in Table 3 were harnessed for the purpose of modeling the fuel cells, encompassing the pertinent nominal data corresponding to the fuel cell under study. It was discerned during the preliminary stage that the nominal model would diverge from the models applied in current operational scenarios for the fuel cells.

Table 3. Fuel cell system parameters adopted for modeling as reference values.

Parameter	Symbol	System HEL
Open circuit voltage	E_{oc}	0.66
Activation overvoltage	A	0.056
Area-specific resistance	r	0.2
Constants in the mass-transfer overvoltage	m	1E-6
Constants in the mass-transfer overvoltage	n	28
Active area of stock	a_{st}	150
Number of cells in the fuel stack	n_{st}	36

6. Testing of Cells under Static and Dynamic Conditions

The characteristics of the fuel cell stack were determined based on the recorded values of voltage and current generated by the fuel cell. The cell temperature values were in the range of 41–55°C (the initial stack temperature was 50°C). The voltage-current characteristics of the cells operating in two cases (static/dynamic) are included in Fig. 3. Due to the nature of the load for the static path, the points are concentrated in three areas of the voltage-current characteristics. The spread of values in the mentioned areas is due to the difference between the actual and set current values. It should be noted that the dynamic characteristics partially overlap with the points of the static characteristics. Dynamic characteristics have two types of changes: one with smaller voltage values at the same current values relates to increasing the load, while the other relates to decreasing the load. The characteristic with the smallest voltage values was formed first, with the smallest value of the cell temperature. It follows that the static characteristics coincide with the conditions for reducing the power of the fuel cell (reducing its load). All voltage-current characteristics during load increase are practically the same.

For both characteristics, the power curve was also

determined as an interpolation of the points relating to the voltage-current characteristics. Figure 3 shows the same power curve characteristics for both load variants.

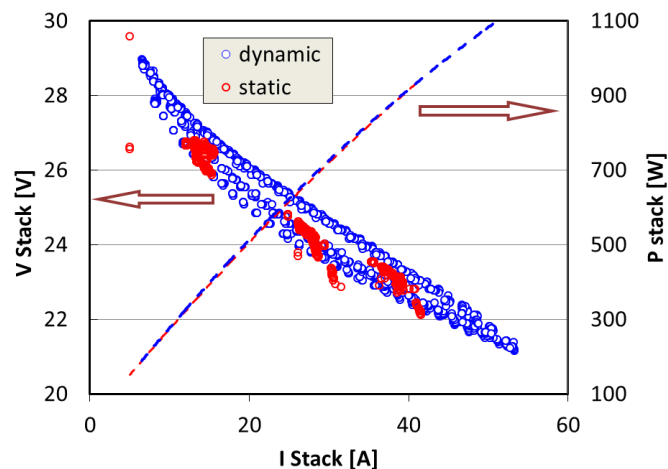


Fig. 3. Characteristics of the fuel cell stack: voltage-current and power characteristics in two operating states: static and dynamic.

The analysis of the power and efficiency values of the fuel cell stack was carried out according to the following methodology. Taking into account the values of U_{FC} cell voltage, I_{FC} cell current, current to supply the I_{FC_Op} cell system and H_{2n} hydrogen flow rate according to Figure 1b, the following values were determined:

- fuel cell power

$$P_{FC} = U_{FC} \cdot I_{FC} \text{ [W]} \quad (7)$$

- fuel cell module power

$$P_{FCM} = U_{FC} \cdot (I_{FC} - I_{FC_Op}) \text{ [W]} \quad (8)$$

- hydrogen power

$$P_{H_2} = \frac{H_{2n}}{60} \cdot H_U \text{ [W]} \quad (9)$$

- stack efficiency

$$\eta_{FC} = \frac{P_{FC}}{P_{H_2}} \quad (10)$$

- fuel cell module efficiency

$$\eta_{FCM} = \frac{P_{FCM}}{P_{H_2}} \quad (11)$$

- converter DC/DC efficiency

$$\eta_{DC/DC} = \frac{P_{OUT}}{P_{FCM}} \quad (12)$$

where P_{OUT} is the power at the output of the DC/DC voltage converter.

According to equation (12), the efficiency of the voltage converter was determined (Fig. 4). This efficiency is highest

during low loads on the fuel cell stack and obtains a value of about 0.97. As the load on the cell increases, the converter efficiency decreases to about 0.94. Smaller values of the converter efficiency were not observed.

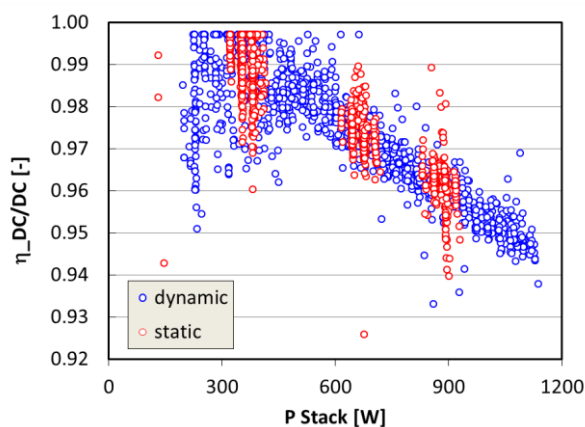


Fig. 4. Characteristics of the efficiency of the DC/DC voltage converter with respect to the power of the fuel cell stack: in two states of operation: static and dynamic.

7. Fuel Cell Stack Efficiency Analysis

The power curve of the single fuel cell stack and the entire FCM module is shown in Fig. 5. Changes in the temperature values of the fuel cell stack are also included (dashed blue

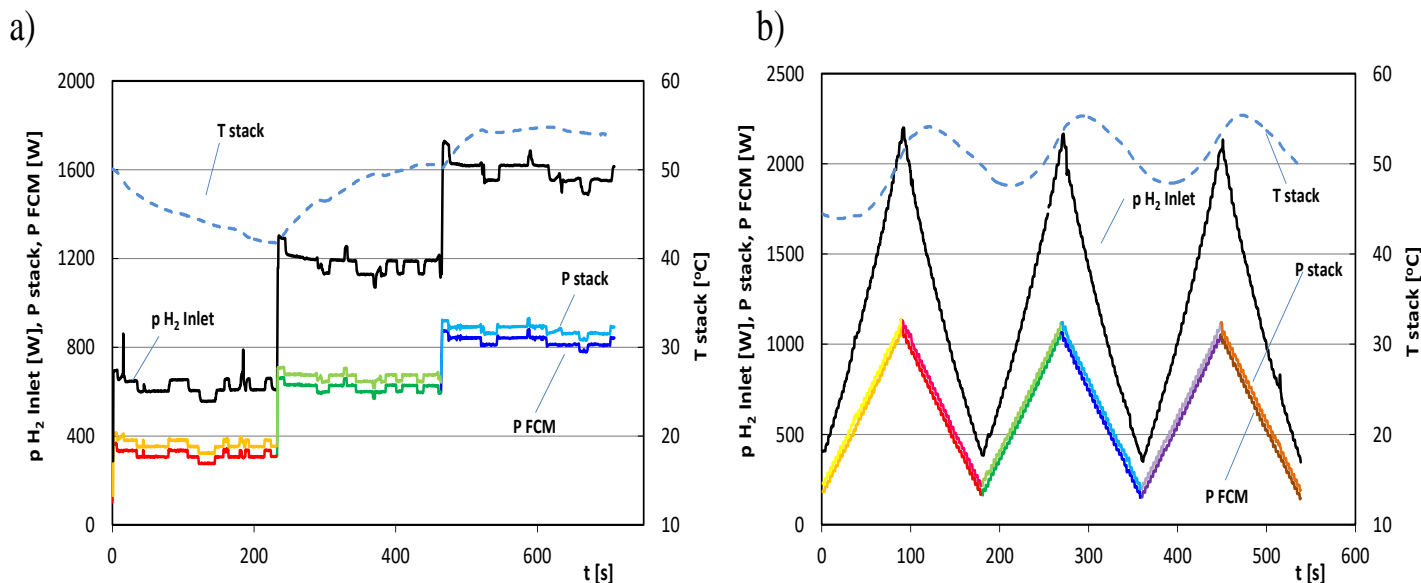


Fig. 5. Performance characteristics of the fuel cell stack: a) under static conditions, b) under dynamic conditions.

Considering equations (10) and (11), the efficiency of the fuel cell stack itself and the FCM module were determined. The results of these analyses are shown in Fig. 6. Static loading of the fuel cells results in fuel cell efficiency of 55–60%. These values are slightly higher at the beginning of the

line). In static tests, the temperature at the beginning of the tests was 50°C. With a constant load, it decreased to a value of 40°C. Subsequent increases in load caused the temperature to rise to about 55°C. Keeping the load values of the cell constant results in a change in temperature depending on the load. It follows that air cooling is effective, but the stack temperature reaches a maximum value of 55°C. During dynamic testing, the temperature changes periodically with changes in load.

The power of the fuel cell stack and the fuel cell module were determined according to equations (7) and (8). Due to the I_{FC_op} current (Fig. 1b), the power of the fuel cell module is lower than that of the fuel cell stack. The values of module power reduction are similar during static and dynamic tests (Fig. 5a and 5b). Under static conditions, the value of cell power lost to cell operation (P_{FC_op}) averages 45 W. Under dynamic conditions, these losses amount to a minimum of: 54 W and the maximum values reach about 63 W. This means that under dynamic loading conditions, the cell operating power is about 20% higher than during static testing.

test and decrease with increasing load values. The efficiency of the fuel cell module is several percentage points lower. This reduction is proportional to the load value. In the initial phase at low load, the differences between the efficiency are about 8%. At the highest load value, the differences decrease to

a value of about 3%. The process of anode purge disturbs the normal values of the determined efficiency and should not be analyzed as a value that appears cyclically. When realizing the dynamic load profile during a rapid increase in load, a reduction in the efficiency of the fuel cell stack and the fuel

cell module was observed. The dynamics of the fuel cell operation results in larger efficiency differences being obtained. At maximum load, efficiencies of around 65 were obtained, while decreasing load resulted in a drop in efficiency to around 40%.

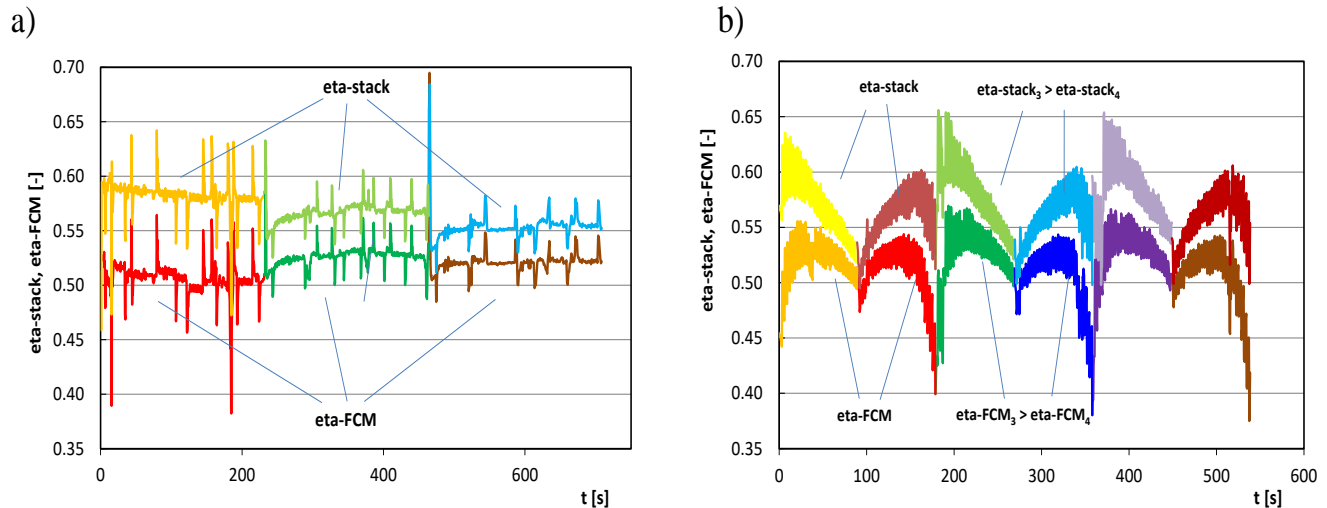


Fig. 6. Efficiency characteristics as a function of time for the fuel cell stack and FCM module: a) under static conditions, b) under dynamic conditions.

The foregoing analyses do not allow indicating the best efficiency of the cell with respect to load. In the next stage of the research work (Fig. 7), the efficiency of the fuel cell stack and FCM module was determined in relation to the energy supplied in the hydrogen form. According to equation (9), the hydrogen flow rate is proportional to the power delivered with hydrogen. Under static conditions, the highest fuel cell efficiency is obtained at a flow rate of about 3–4 nl/min. The power of the FCM is practically independent of the hydrogen

flow rate under these conditions. Tests under dynamic conditions, due to the wide variety of test points, make it possible to determine the optimal conditions (highest efficiency from hydrogen flow rate). With regard to the fuel cell stack, the maximum efficiency value falls in the flow range of about 5 nl/min. For the fuel cell module, the range of maximum efficiency shifts toward higher flow rates. The maximum efficiency is reached at about 8 nl/min.

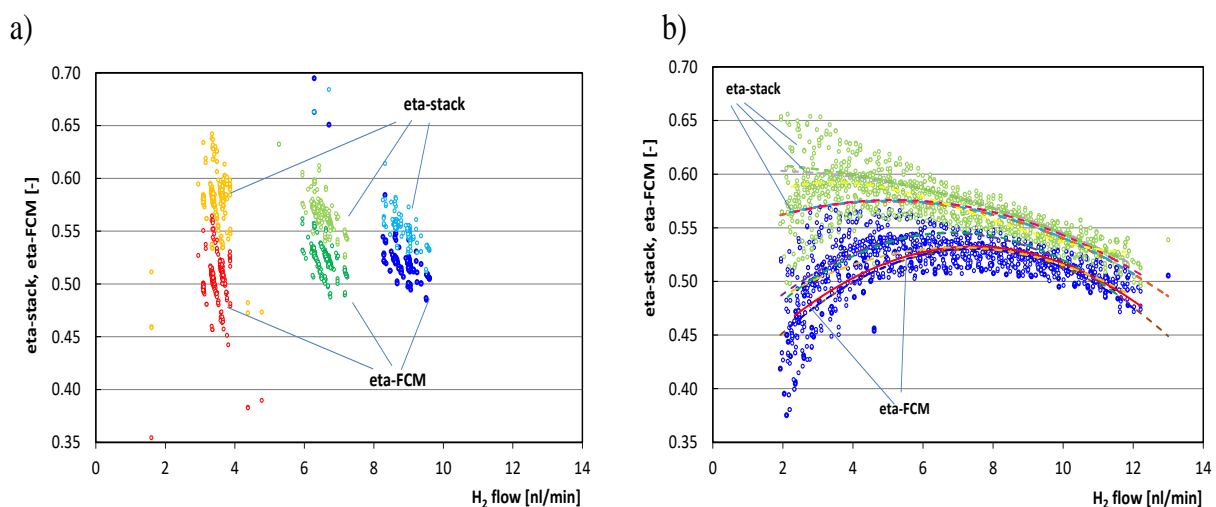


Fig. 7. Efficiency characteristics as a function of hydrogen consumption for the fuel cell stack and FCM module: a) under static conditions, b) under dynamic conditions.

Figure 8 shows the energy balance of an FCM module operating according to a static load profile. The lower part of the figure contains percentages, while the upper part contains values expressed in terms of power mostly calculated from voltage and current measurements (except for stack heat). The points of operation at 100, 300 and 600 seconds after the start of the load profile, that is, the minimum, average and maximum load on the system, were selected for analysis. The largest share of losses in the overall balance is thermal (calculated) losses, whose value increases with load. This is

due to the heating of the stack as the load increases. Another component of the balance is the energy devoted to the operation of the stack, i.e. supplying fuel to the anode or pumping air into the open cathode, for example. In the overall balance, the share of FC operation energy is small and decreases with load, due to the facts of the necessity of functioning of system actuators regardless of load. Losses devoted to DC/DC converter operation and system operation contribute the least to the entire balance and their value is practically constant regardless of the load.

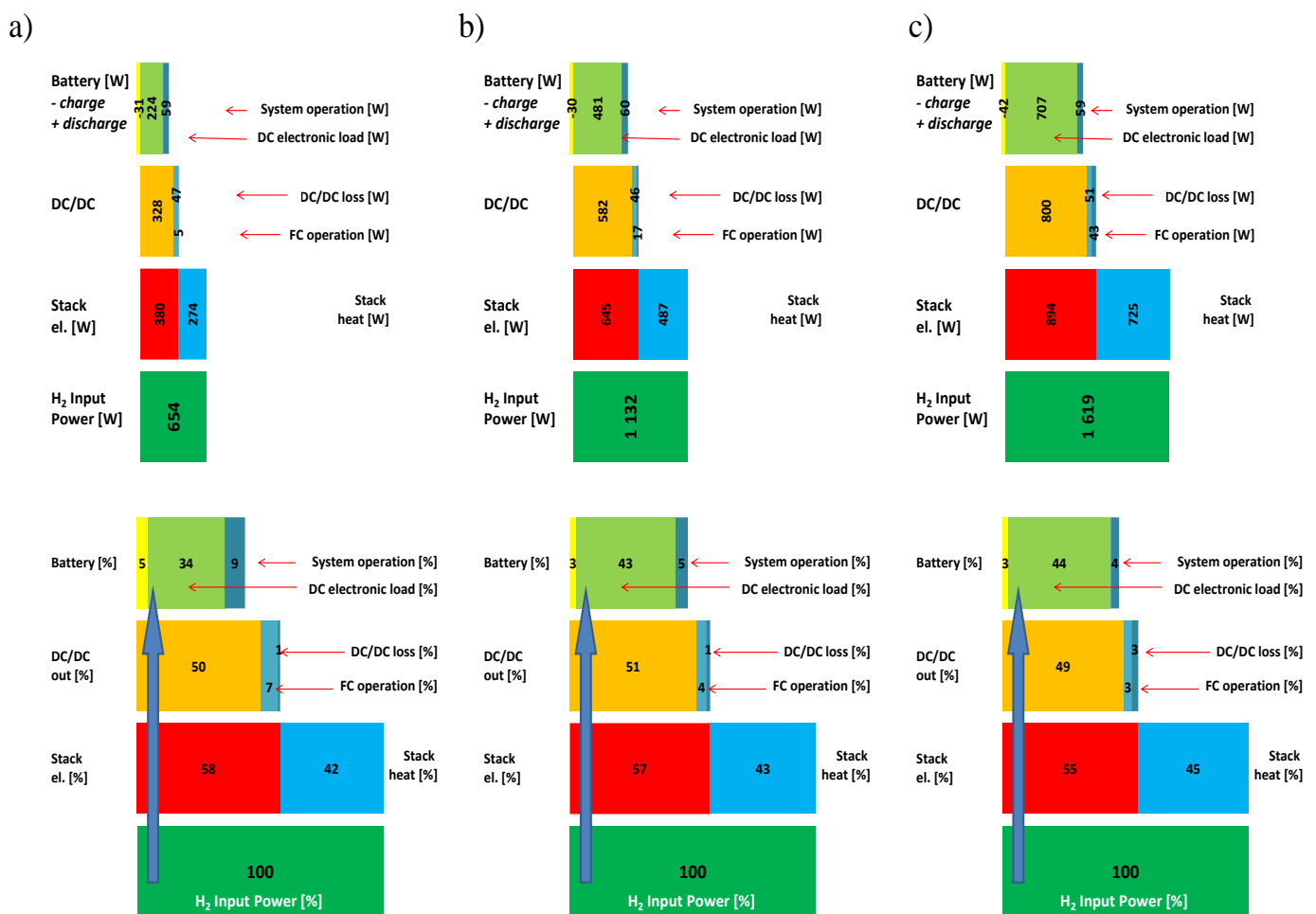


Fig. 8. Sankey diagrams (heat distribution in a fuel cell in static tests at specific time conditions: a) at $t = 100$ s; b) at $t = 300$ s, c) at $t = 600$ s

The energy balance for the dynamic load profile (Fig. 9) was compiled for points 15, 30 and 90 seconds after the start of the load profile. At 90 seconds, the load increased from 114 to 849 W. In the case of dynamic versus static changes, the differences in heat loss do not present a clear trend and the minimum value is reached after 30 seconds of operation. This is probably due to the heating delay of the stack. The largest

share of heat loss is reached at the highest load as is the case with static loading. Under dynamic conditions, a larger share relative to static conditions was recorded for FC operation. This is due to the increased intensity of operation of the actuators handling the fuel cell stack. As for the DC/DC converter, regardless of the operating conditions, energy losses are marginal.

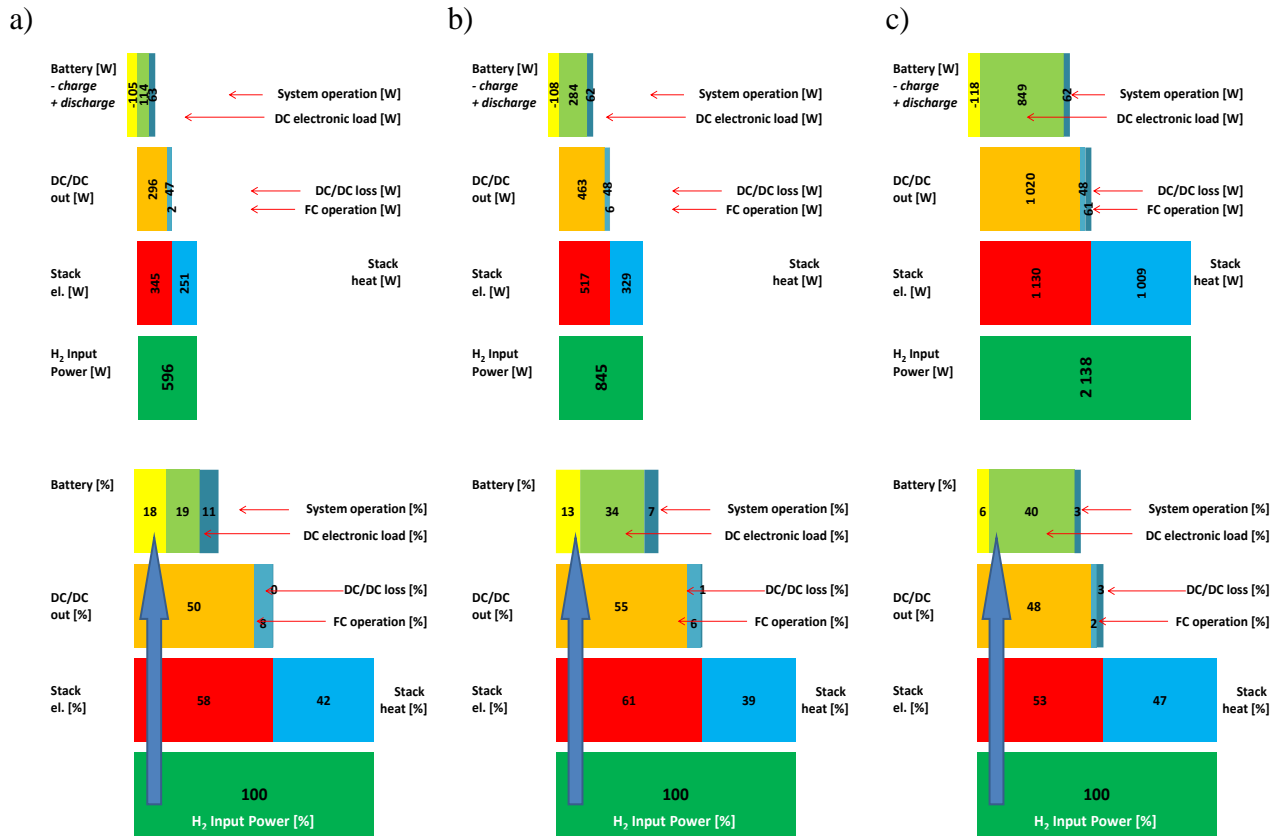


Fig. 9. Sankey diagrams (heat distribution in a fuel cell) in dynamic tests under specific time conditions: a) at $t = 15$ s; b) at $t = 30$ s, c) at $t = 90$ s.

8. Fuel Cell Modeling

Fuel cell modeling was conducted according to the equations presented in section 3. Equations were selected to include all fuel cell losses. The modeling of fuel cells relied on the pursuit of the minimum value of the objective function:

$$\sum(U_{st} - U_m)^2 \rightarrow \min \quad (13)$$

where U_{st} – research voltage values in the fuel cell stack, U_m – the consecutive values of model voltage.

Accordingly, Table 4 contains the quantities necessary for fuel cell modeling. The table assumes default values set by the fuel cell manufacturer (column "HEL system – default"). For such values, the criterion value specified in equation (13) was

determined. With such adoption of the values necessary to determine the sum of squares, the voltage waveform shown in Figure 10 was obtained. For the default values, results were obtained as shown in Table 4 and Figure 10. These results significantly deviate from the operating values. In static conditions, the maximum difference between the operating voltage and the default model is about 3.8 V. In dynamic conditions, this value is much smaller at 2.05 V. This is due, among other things, to the typical operation of fuel cells – they degrade. At the same time, as a result of an operation, fuel cell losses also increase. Information about such changes is short-circuited, among others, in publications [29–33].

Table 4. Fuel cell system parameters adopted for modeling as reference values.

Symbol	System HEL – default	Static model	Dynamic model
E_{oc}	6.60E-01	6.36E-01	6.59E-01
A	5.60E-02	5.89E-02	5.50E-02
r	2.00E-01	2.08E-01	4.69E-01
m	1.00E-06	7.96E-07	5.41E-03
n	2.80E+01	2.68E+01	1.12E-01
a_{st}	1.50E+02	1.43E+02	2.17E+02
n_{st}	3.60E+01	3.49E+01	3.46E+01
$\sum(U_o - U)^2$ – default		3119.11	1992.92
$\sum(U_o - U)^2$ – fit model		55.66	136.44

As a result of the procedures used for minimizing the objective function, parameter values (included in Table 4) were obtained for the static and dynamic model, respectively. For the static model, the criterion reached a value of 55.66 V^2 (in the default conditions – 3119.11 V^2), while for the dynamic model, 136.44 V^2 (1992.92 V^2) was obtained.

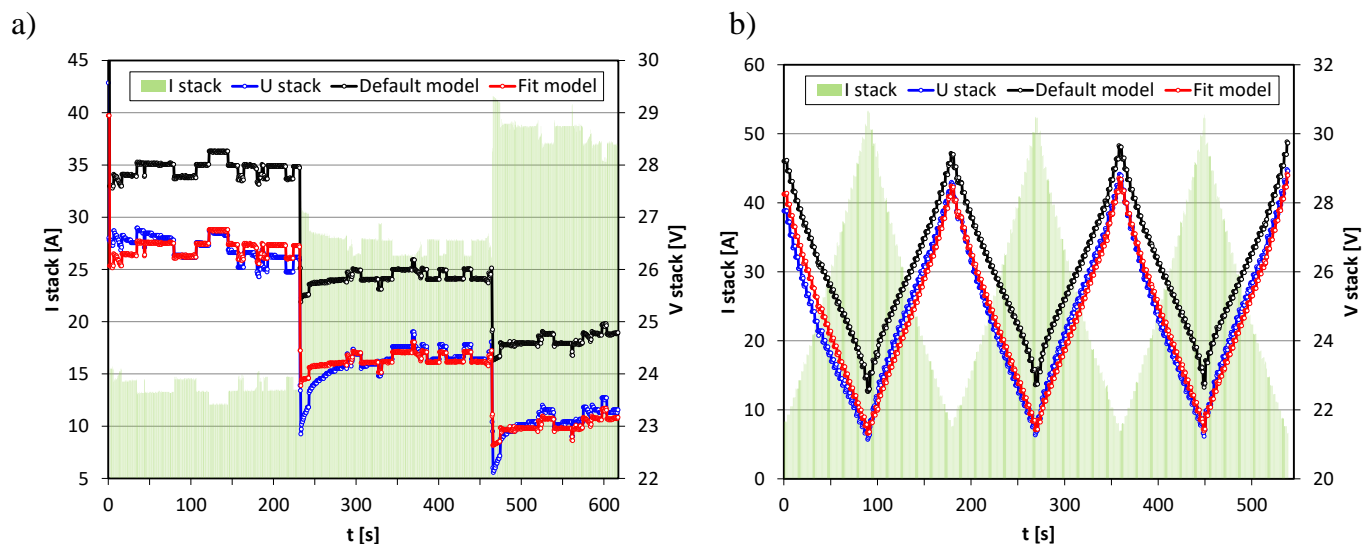


Fig. 10. Fuel cell models vs. experimental results: a) under static conditions, b) under dynamic conditions.

9. Summary

The presented modeling and experimental investigation were aimed at characterizing the performance of the hybrid fuel cell stack system under static and dynamic loading conditions. It was found that the rate of change of the load has a direct effect on the course of the current-voltage characteristics of the stack. In terms of experimental research, it was found that:

1. As the stack power increases, a decrease in the efficiency of the DC/DC voltage converter is observed regardless of static or dynamic conditions; however, these changes are in the range up to $\eta = 0.94$ and reach higher values for static changes
2. The conditions of dynamic change in the load of the cell result in obtaining maximum stack efficiency around $\eta = 0.6-0.65$ at a fairly low rate of hydrogen consumption (2–3 nl/min).

The Sankey energy balance created for the system's static load profile indicates that the system's energy is distributed,

Acknowledgements

This work was supported by the statutory work 0451/SBAD/0342 and 0451/SBAD/0343 (Poznan University of Technology).

It should be noted that the values of the dynamic model parameters are sometimes significantly different than during the adopted static model values. When analyzing the results in Fig. 10, it can be seen that the small differences in cell current ΔI despite dynamic conditions result in smaller unit deviations ($-0.5 \text{ V}; +0.75 \text{ V}$) than during static tests ($-0.6 \text{ V}; +2.38 \text{ V}$).

but the distribution is highly dependent on the cell's load: despite load differences, the cell's efficiency did not fall below 51% (at hydrogen power values of more than 1600 W). Dynamic conditions at similar hydrogen powers are characterized by similar values of stack efficiency.

In terms of modeled studies, it was found that:

1. It is possible to model fuel cells' static and dynamic operation using known models.
2. Significantly better results (fit) are obtained with static modeling of fuel cells; the parameters of static and dynamic models obtain quite large discrepancies but allow fairly accurate modeling.

The experimental studies and modeling of the low-power fuel cell stack make it possible to predict the ageing changes of high-power fuel cells (so-called scaling). Thus, the above studies become a prelude to determining the ageing changes of fuel cells used in FC vehicles (with a power of about 100 kW) during tests under real driving conditions.

References

1. Wee J-H. Applications of proton exchange membrane fuel cell systems. *Renewable and Sustainable Energy Reviews*. 2007;11(8):1720-1738. <https://doi.org/10.1016/j.rser.2006.01.005>
2. Di Giorgio P, Di Ilio G, Scarpati G, Erme G, Simeoni E, Jannelli E. Design of a hydrogen-powered bicycle for sustainable mobility. *E3S Web of Conferences*. 2022;334:06012. <https://doi.org/10.1051/e3sconf/202233406012>
3. Boukoberine MN, Zia MF, Benbouzid M, Zhou Z, Donateo T. Hybrid fuel cell powered drones energy management strategy improvement and hydrogen saving using real flight test data. *Energy Conversion and Management*. 2021;236:113987. <https://doi.org/10.1016/j.enconman.2021.113987>
4. Miller AR, Hess KS, Barnes DL, Erickson TL. System design of a large fuel cell hybrid locomotive. *Journal of Power Sources*. 2007;173(2):935-942. <https://doi.org/10.1016/j.jpowsour.2007.08.045>
5. Switch. Sea Change. July 2023. Retrieved from, <https://www.switchmaritime.com/projects>
6. Fuel cell combined heat & power (CHP) system/stationary fuel cell power generator. July 2023. Retrieved from, <https://en.huadehydrogen.com/Pure-Hydrogen-Fuel-Cell-CHP-System-pl3811699.html>
7. Hoeflinger J, Hofmann P. Air mass flow and pressure optimisation of a PEM fuel cell range extender system. *International Journal of Hydrogen Energy*. 2020;45(53):29246-29258. <https://doi.org/10.1016/j.ijhydene.2020.07.176>
8. Sveshnikova A, Marcobertardino GD, Pirrone C, Bischì A, Valenti G, Ustinov A, Campanari S. The impact of humidification temperature on a 1 kW proton exchange membrane fuel cell stack. *Energy Procedia*. 2017;142:1661-1667. <https://doi.org/10.1016/j.egypro.2017.12.546>
9. Loskutov A, Kurkin A, Shalukho A, Lipuzhin I, Bedretdinov R. Investigation of PEM fuel cell characteristics in steady and dynamic operation modes. *Energies*. 2022;15:6863. <https://doi.org/10.3390/en15196863>
10. Yang Y, Jia H, Liu Z, Bai N, Zhang X, Cao T, Zhang J, Zhao P, He X. Overall and local effects of operating parameters on water management and performance of open-cathode PEM fuel cells. *Applied Energy*. 2022;315:118978. <https://doi.org/10.1016/j.apenergy.2022.118978>
11. Yan Q, Toghiani H, Causey H. Steady state and dynamic performance of proton exchange membrane fuel cells (PEMFCs) under various operating conditions and load changes. *Journal of Power Sources*. 2006;161(1):492-502. <https://doi.org/10.1016/j.jpowsour.2006.03.077>
12. Cieřliński J, Kaczmarczyk T, Dawidowicz B. Dynamic characteristics of the proton exchange membrane fuel cell module. *Archives of Thermodynamics*. 2018;39(4):125-140. <https://doi.org/10.1515/aoter-2018-0033>
13. Chandran M, Palaniswamy K, Karthik Babu NB, Das O. A study of the influence of current ramp rate on the performance of polymer electrolyte membrane fuel cell. *Sci Rep*. 2022;12:21888. <https://doi.org/10.1038/s41598-022-25037-0>
14. Huang Z, Shen J, Chan SH, Tu Z. Transient response of performance in a proton exchange membrane fuel cell under dynamic loading. *Energy Conversion and Management*. 2020;226:113492. <https://doi.org/10.1016/j.enconman.2020.113492>
15. Ma T, Cong M, Wang Y, Liang Y, Wang K, Yang Y. Investigation of PEM fuel cell degradation under on-off cyclic condition. *SAE Technical Paper* 2021. 2021-01-7022. <https://doi.org/10.4271/2021-01-7022>
16. Huang Z, Shen J, Chan SH, Tu Z. Transient response of performance in a proton exchange membrane fuel cell under dynamic loading. *Energy Conversion and Management*. 2020;226:113492. <https://doi.org/10.1016/j.enconman.2020.113492>
17. Kumar R, Subramanian KA. Enhancement of efficiency and power output of hydrogen fuelled proton exchange membrane (PEM) fuel cell using oxygen enriched air. *International Journal of Hydrogen Energy*. 2023;48(15):6067-6075. <https://doi.org/10.1016/j.ijhydene.2022.11.141>
18. Liu P, Xu S. Experimental analysis of -30°C cold start process for an automotive PEM fuel cell system. *SAE Technical Paper* 2022. 2022-01-0694. <https://doi.org/10.4271/2022-01-0694>
19. Walters M, Wick M, Tinz S, Ogrzewalla J, Sehr A, Pischinger S. Fuel cell system development: a strong influence on FCEV performance. *SAE Int J Alt Power*. 2018;7(3):335-350. <https://doi.org/10.4271/2018-01-1305>
20. Vidović T, Tolj I, Radica G, Bodrožić Coko N. Proton-exchange membrane fuel cell balance of plant and performance simulation for vehicle applications. *Energies*. 2022;15:8110. <https://doi.org/10.3390/en15218110>

21. Sery J, Leduc P. Fuel cell behavior and energy balance on board a Hyundai Nexu. *International Journal of Engine Research*. 2022;23(5):709-720. <https://doi.org/10.1177/14680874211059046>
22. Wang H, Gaillard A, Hissel D. A review of DC/DC converter-based electrochemical impedance spectroscopy for fuel cell electric vehicles. *Renewable Energy*. 2019;141:124-138. <https://doi.org/10.1016/j.renene.2019.03.130>
23. Pietra A, Gianni M, Zuliani N, Malabotti S, Taccani R. Experimental characterization of a PEM fuel cell for marine power generation. *E3S Web of Conferences*. 2022;334:05002. <https://doi.org/10.1051/e3sconf/202233405002>
24. Verry WD. DC-DC converter topology in a 5 kW PEM fuel cell. 2014 IEEE 36th International Telecommunications Energy Conference (INTELEC). 2014:1-8. <https://doi.org/10.1109/intlec.2014.6972145>
25. Barbir F. Fuel cell electrochemistry (chapter 3), Editor(s): Frano Barbir, PEM Fuel Cells. Academic Press, 2005. 33-72. <https://doi.org/10.1016/B978-012078142-3/50004-5>
26. Larminie J, Dicks A. Fuel cell systems explained. Third Edition. John Wiley & Sons Ltd; 2018. <https://doi.org/10.1002/9781118706992>
27. Hybrid Energy Lab. Instruction Heliocentris Academia GmbH. 2016. <http://www.heliocentris.com>
28. Kandidayeni M, Chaoui H, Boulon L, Kelouwani S, Trovão JPF. Online system identification of a fuel cell stack with guaranteed stability for energy management applications. *IEEE Transactions on Energy Conversion*. 2021;36(4):2714-2723. <https://doi.org/10.1109/TEC.2021.3063701>
29. Pielecha I. Modeling of fuel cells characteristics in relation to real driving conditions of FCHEV vehicles. *Energies*. 2022;15:6753. <https://doi.org/10.3390/en15186753>
30. Yuvarajan S, Yu D. Characteristics and modelling of PEM fuel cells. 2004 IEEE International Symposium on Circuits and Systems (ISCAS). 2004:880-883. <https://doi.org/10.1109/ISCAS.2004.1329949>
31. Gong C, Xing L, Liang C, Tu Z. Modeling and dynamic characteristic simulation of air-cooled proton exchange membrane fuel cell stack for unmanned aerial vehicle. *Renewable Energy*. 2022;188:1094-1104. <https://doi.org/10.1016/j.renene.2022.02.104>
32. Bai F, Lei L, Zhang Z, Li H, Yan J, Chen L, Dai Y-J, Chen L, Tao W-Q. Application of similarity theory in modeling the output characteristics of proton exchange membrane fuel cell. *Int J Hydrogen Energy*. 2021;46(74):36940-36953. <https://doi.org/10.1016/j.ijhydene.2021.08.205>
33. Ceran B, Orłowska A, Krochmalny K. The method of determining PEMFC fuel cell stack performance decrease rate based on the voltage-current characteristic shift. *Eksploatacja i Niezawodność*. 2020;22(3):530-535. <https://doi.org/10.17531/ein.2020.3.16>